crystals

MDPI

Article

Novel Devices for Transporting Protein Crystals to the Synchrotron Facilities and Thermal Protection of Protein Crystals

Andrea Flores-Ibarra [1], Camila Campos-Escamilla [1], Yasel Guerra [2], Enrique Rudiño-Piñera [2], Nicola Demitri [3], Maurizio Polentarutti [3], Mayra Cuéllar-Cruz [4] and Abel Moreno [1,*]

1 Instituto de Química, Universidad Nacional Autónoma de México, Av. Universidad 3000, UNAM, 04510 Ciudad de México, México; andreafi@outlook.com (A.F.-I.); camila.cescamilla@gmail.com (C.C.-E.)
2 Departamento de Medicina Molecular y Bioprocesos, Instituto de Biotecnología, Universidad Nacional Autónoma de México, Avenida Universidad 2001, Colonia Chamilpa, 62210 Cuernavaca Morelos, Mexico; yaselg@ibt.unam.mx (Y.G.); rudino@ibt.unam.mx (E.R.-P.)
3 Elettra—Sincrotrone Trieste, S.S. 14 km 163.5 in Area Science Park, 34149 Basovizza-Trieste, Italy; nicola.demitri@elettra.eu (N.D.); maurizio.polentarutti@elettra.eu (M.P.)
4 Departamento de Biología, División de Ciencias Naturales y Exactas, Campus Guanajuato, Universidad de Guanajuato, Noria Alta S/N C.P., 36050 Guanajuato, México; cuellarmay@yahoo.com.mx
* Correspondence: carcamo@unam.mx; Tel.: +52-55-56224467

Received: 10 August 2018; Accepted: 20 August 2018; Published: 23 August 2018

Abstract: In this article, we use novel and non-conventional devices, based on polyolefins that help to increase the thermal protection of protein crystals in their crystallization conditions for crystallographic applications. The present contribution deals with the application of some ad hoc devices designed for transporting protein crystals to the synchrotron facilities. These new devices help transporting proteins without cryo-cooling them, therefore replacing the conventional dry Dewars. We crystallized four model proteins, using the classic sitting-drop vapor diffusion crystallization setups. The model proteins lysozyme, glucose isomerase, xylanase, and ferritin were used to obtain suitable crystals for high-resolution X-ray crystallographic research. Additionally, we evaluated the crystallization of apo-transferrin, which is involved in neurodegenerative diseases. As apo-transferrin is extremely sensitive to the changes in the crystallization temperature, we used it as a thermal sensor to prove the efficiency of these thermal protection devices when transporting proteins to the synchrotron facilities.

Keywords: lysozyme; glucose isomerase; xylanase; ferritin; insulin; apo-transferrin; crystal growth in solution; gel-growth; conventional and non-conventional methods of protein crystallization

1. Introduction

Currently, X-ray biocrystallography is one of the most powerful tools for obtaining the three-dimensional (3D) structure of some rather special target molecules. However, well-diffracting crystals are mandatory in order to obtain the 3D structure, so they can be applied in life sciences and biomedical research [1,2]. These X-ray diffraction techniques are not the only way to obtain the 3D structure of biological macromolecules [3–11]. In spite of all the different methods available for obtaining the 3D structures, we have yet a lot to learn from the investigations based on the crystallogenesis research of proteins [12,13]. The chemical properties of protein solutions such as the chemical potential (driving force in protein crystallization), ionic strength (concentrations of reactants), pH values to play with the isoelectric point of proteins [14] as well as their physical parameters like pressure and temperature are still poorly explored [14–16].

At present, we have not many investigations that deal with the role of temperature for protein crystallization [17–21], though we still find a few. Budayova-Spano et al., have developed new strategies and devices to grow big crystals for neutron diffraction [22], and for protein crystallization using buttons of dialysis [23,24]. Vessler et al., have even considered the temperature as a practical physicochemical parameter to play around the solubility diagram for growing, dissolving, and controlling the size and shape of some protein crystals [25,26]. We also find some screenings for cycling temperature strategies to improve the crystallization efficiency [27], as well as approaches based not only on controlling the temperature in small droplets (like the TG40 device developed by Juárez-Martinez et al.) [28], but also controlling the humidity when collecting X-ray data in situ [29]. However, the use of temperature to search for different polymorphs in protein crystallization research has rarely been explored [18,30,31].

On the other hand, we have apo-transferrins, which are challenging proteins biomolecules for crystallization and for obtaining high-resolution three-dimensional crystallographic structures, as they are very sensitive to temperature. Apo-transferrins also play an important role in neurodegenerative diseases and a in the transport of iron to the brain [32–35].

In this contribution, we evaluated the thermal protection of proteins by using novel polyolefin-made devices to transport model protein crystals and apo-transferrin crystals to the synchrotron facilities at room temperature. The crystal structure and the electron density maps of the best crystals showed well-defined, and distinctly separated atoms at the selected aromatic residues, as indicators of the highest X-ray protein crystal-quality. We used human transferrins, not only for their implication in neurodegenerative disorders, but also for their role as thermal sensors. Transferrins are extremely sensitive to the changes in the crystallization temperature. This contribution deals with the importance of temperature control to avoid damaging protein crystals when being transported to synchrotron facilities. These thermal protection devices are promising containers for transporting, and protecting biological macromolecules for X-ray data collection at the synchrotron facilities, substituting the conventional dry Dewars.

2. Materials and Methods

2.1. Protein Crystallization Conditions and Cryo-Protection

The first model protein used for these experiments was lysozyme (Seikagaku Co., Minato-ku, Tokyo.); the second was glucose isomerase (Hampton Research Corporation, Aliso Viejo, CA, USA); the third model protein was xylanase (Hampton Research Corporation Ca. No. HR7-104); and the final fourth was ferritin from horse spleen (Sigma, St. Louis, MS, USA). All these proteins were crystallized using the classical sitting drop vapor-diffusion set up, fixed at 18 °C. The droplets of 2 µL were gently mixed 1:1 protein and precipitating agent, the well of Qiagen plates was filled with 500 µL whereas the plates of 96 wells and the disposables plastic inserts of the TG40 were filled with 40 µL. For lysozyme a solution of 120 mg/mL was prepared in 100 mM sodium acetate buffer pH 4.5. The precipitating agent, 60 mg/mL NaCl, was prepared using the same buffer solution. For glucose isomerase the crystallization conditions consisted of a typical protein concentration of 30 mg/mL and, as precipitating agent, we used 200 mM ammonium acetate buffer pH 7.0, 30% (*w*/*v*) PEG 6000. In the case of xylanase, it had to be prepared prior to crystallization by diluting the stock solution (36 mg/mL) with sterile filtered deionized water. The precipitating agent was a mixture of ammonium sulfate 1.2 M and sodium iodide 1 M. The droplets were prepared 1:1 protein and precipitating agent. We would like to remark that in ammonium sulfate the solubility of xylanase crystals increases exponentially as temperature rises [36]. Finally, the last model protein ferritin (75 mg/mL) was crystallized by mixing 1:1 protein and precipitating agent (0.8 M ammonium sulfate prepared in 100 mM Tris-HCl pH 7.5 and 60 mM cadmium sulfate). In the case of lysozyme, we used as a cryoprotectant 30% (*v*/*v*) PEG-1000 mixed with mother liquor of NaCl (precipitating agent), however, for this particular protein, lower concentrations of its cryo-protectant (in this case NaCl/PEG-1000 and mother liquor) proved not to

be efficient since the crystals were dissolved and damaged. Consequently, ice rings were observed in lower concentrations of this cryo-protectant. In the case of glucose isomerase, the best cryo-protectant was its own precipitating agent. For the rest of the proteins the cryo-solution was prepared by mixing the precipitating agent with 30% (*v/v*) glycerol.

Particularly, apo-transferrin was purchased with a purity of 98%. Lyophilized human serum apo-transferrin (Sigma-Aldrich, St. Louis, MO, USA) reconstituted in 50 mM Tris-HCl pH 8.0, and 20 mM Na_2CO_3, at a protein concentration of 5 mg/mL. The protein was applied to a 5 mL anion exchange HiTrap Q HP column (GE Healthcare Life Sciences, Chicago, IL, USA), attached to a fast protein liquid chromatography (FPLC) system (Pharmacia, Pfizer, NJ, USA), and equilibrated with 50 mM Tris-HCl pH 8.0, and 20 mM Na_2CO_3. The protein was eluted using a linear gradient from 0 to 150 mM NaCl over 4 column volumes. Peak fractions of the protein were pooled and dialyzed overnight into 20 mM Tris-HCl pH 8.0, 20 mM Na_2CO_3 and 200 mM NaCl. In order to crystallize the apo-transferrin, the protein was centrifuged at a controlled temperature in a DuPont centrifuge using an Amicon Ultra-15 Ultracel-5k tube (Millipore, Burlington, MA, USA) to a protein concentration of 30 mg/mL. Crystals were obtained by sitting-drop vapor diffusion technique with a well solution of PEG/Ion Screen #48 (Hampton Research, Aliso Viejo, CA, USA) consisting of 0.2 M ammonium citrate, and 20% (*w/v*) PEG 3350, adjusted to a pH 7. In order to find the best temperature for the crystallization of apo-transferrin, we fixed 8 crystallization experiments at 5 different temperatures, ranging from 12 to 20 °C (increasing in 2 °C increments)—using a TG40 apparatus (Centeo BioSciences-Blacktrace, Royston, UK). Different temperatures were carefully tested, being the 18 °C the one yielding the best crystals. The apo-transferrin crystals were cryoprotected with 50% (*w/v*) trehalose solution (Sigma Aldrich; St. Louis, MO, USA) mixed 1:1 with the precipitating agent.

2.2. Crystal Growth Devices

As most proteins are sensitive to changes in temperature, there is basically a specific range of very few degrees where protein crystals can keep stable and suitable for crystallization. Phase diagrams are generally very useful to improve the crystallization conditions. However, these diagrams are not always available for the majority of proteins [13–16]. This is why one of the main issues when transporting proteins to synchrotron facilities is temperature (temperature is crucial in the crystallization process). In order to keep a stable low temperature, proteins must be cryo-protected, frozen and transported in dry Dewars following the International Air Transport Association (IATA) procedures for carrying biological crystals. However, on the unfortunate occasions in which we had been revised by some poorly trained custom officers, the Dewars had been opened, and the crystal damaged due to thermal shock. The problem is obvious. In order to prevent future damage of crystals in airport revisions, we worked at designing new devices that will help us to carefully transport them to the synchrotron facilities. These are novel devices made of a patented polymer (polyolefin: US patent US 7,971,744 with a density of 32.04 kg/cm^3), that can resist ranges of temperatures, from −160 °C up to 50 °C, without altering the quality of the protein crystals transported inside. Figures 1–3 show the dimensions of these new devices, which consisted of a rectangular piece of this porous polyolefin with some perforations inside adapted to the conventional and commercially available crystallization plates. The protein crystals, once inside the polymeric devices, are then suitable to be transported even in a regular suitcase without problem. We have already tested these devices by crystallizing some model proteins and transporting them to the synchrotron in terms of checking their efficiency as thermal protectors. The beamline XRD1 of ELETTRA synchrotron located in Trieste Italy, was the facility where the X-ray data collection was performed [37]. Figure 1 shows the first thermal protection device applicable to the 96 well-plates, which are commercially available.

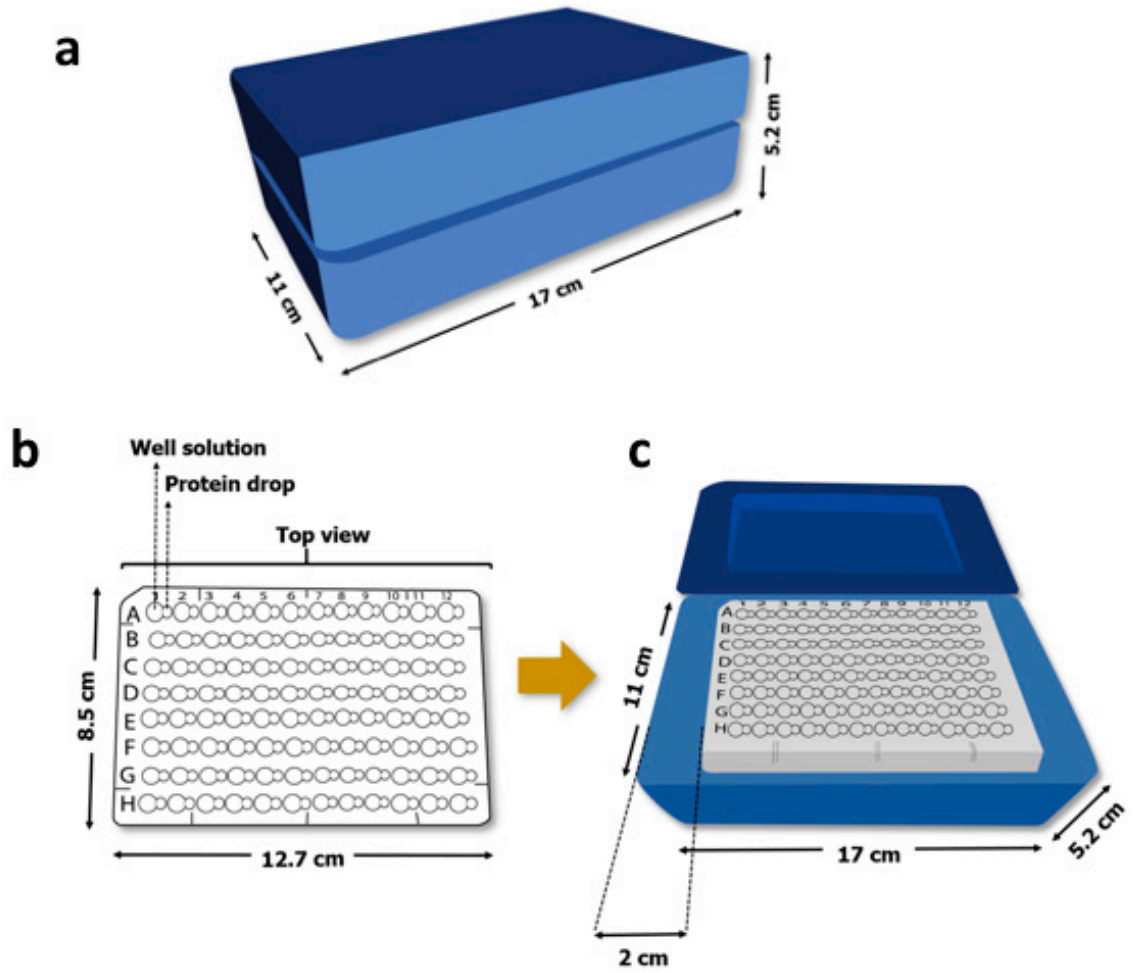

Figure 1. This device can support all types of the conventional plates for vapor diffusion set up in hanging and sitting-drops techniques: (**a**) An overview of the device and dimensions; (**b**) crystallization plate (96 wells) and (**c**) insertion of the crystallization plate.

The second thermal protection device was designed for the crystallization assays, when using a TG40 temperature controller from Centeo Biosciences (Blacktrace Holdings, UK) (Figure 2). The classic vapor diffusion method in a sitting-drop set up is fixed using 40 µL of the mother liquid and drops of 1 µL of protein plus the same amount of precipitating agent. It is important to remark that these plastic disposables inserts are usually closed with adhesive (tape) to prevent evaporation. Basically, the TG40 temperature controller uses plastic disposable inserts that can be introduced in the empty six lanes made on the device (Figure 2). The TG40 allows to fix eight experiments of protein crystallization at five different temperatures at the same time. Once the crystallization experiment is finished the plastic disposables inserts are taken and located into the thermal protection device for transportation. We must emphasize that this device (Figure 2) must be (a) perfectly closed, and (b) transported in vertical position to the synchrotron facility, to avoid leaking of the precipitating agent into the crystallization droplet. The thermal protection devices kept the temperature of the internal part of the crystallization experiment stable during the whole trip. It is important to have stable crystals to obtain a proper X-ray diffraction as shown later on in the results part.

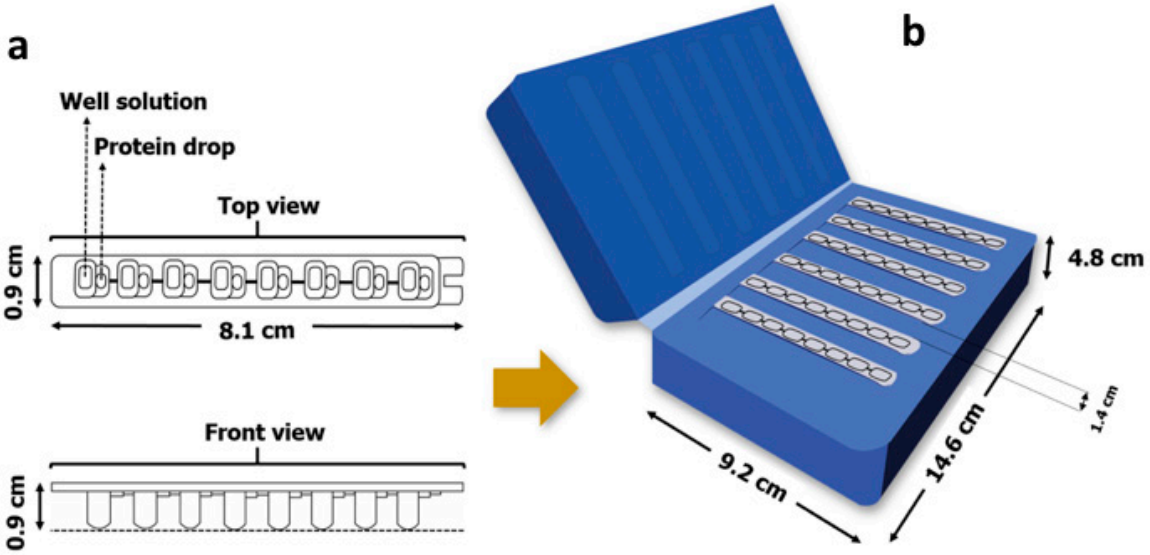

Figure 2. This shows the dimensions and experimental details of the (**a**) top and front view of the plastic disposable inserts used in the TG40 apparatus and (**b**) the general overview and dimensions of the thermal protection device.

The third type of thermal protection device is related to the use of Qiagen plates (formerly called Nextal plates), where the cover slip has a screw system to close the wells properly (Figure 3). A preliminary prototype of these devices for growing crystals in capillary tubes under the presence of strong magnetic fields based on the same polyolefin was evaluated in our previous publication [30].

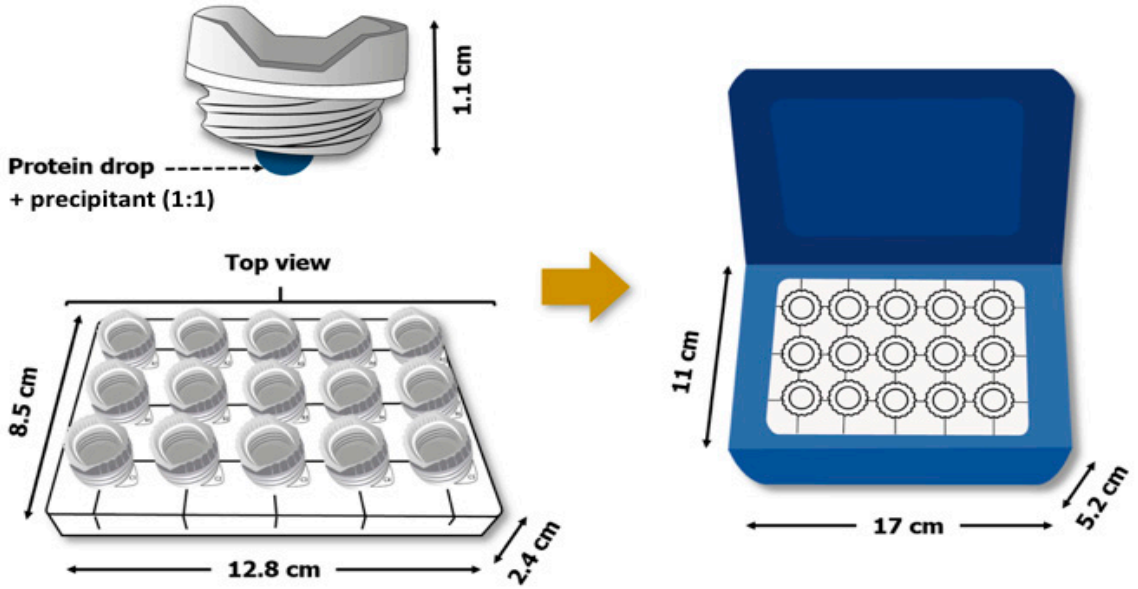

Figure 3. This shows the design of the thermal protection device, when using the Qiagen plates for protein crystallization. On the top left hand-side the cover slip with screw system contains the protein drop mixed with precipitating agent. On the right hand-side the thermal protection device with its dimensions.

All protein crystals were prepared in the best crystallization conditions previously established in the laboratory to get high resolution crystals, except for the case of apo-transferrin, which the maximum resolution reported has been done up to 2.9 Å [32]. Then these crystals were tested at home diffractometer in order to check the maximum diffraction. Afterwards, a set of fresh crystals was prepared following the same procedure, and the samples were transported and diffracted at the synchrotron facility.

2.3. X-ray Data Diffraction and Data Processing

Once the protein crystals were harvested from the solution, they were cryo-protected for X-ray data collection. X-ray diffraction data sets were collected using the X-ray facilities of the synchrotron, with hybrid pixel PILATUS (Dectris, Baden-Daettwil, Switzerland) detector, under cryogenic conditions at 100 K. The crystal-to-detector distance was set to get maximum resolution. Data collection strategies included high redundancy data and each sample was rotated using 0.25° increments. The HKL3000 suite [38], and XDS [39] were used to process, merge, and scale all datasets.

Initial phases for all crystals were determined by molecular replacement with the program Phaser implemented in Phenix platform [40] using the atomic coordinates taken from previously determined data sets in the protein data bank (PDB) (153L, 1MNZ, 3AKP, 4DE6, for lysozyme, glucose isomerase, xylanase and ferritin respectively), after ligands, alternative conformations, heteroatoms and water molecules were refined up to the available resolution. Map inspection, model building, and manual refinement were done with Coot [41] and further rounds of refinement were done with Phenix [42]. Figures were produced using the program PyMol [43].

3. Results and Discussion

We collected the X-ray diffraction of these protein crystals (blanks) at inhouse X-ray facility (Table 1) in order to be compared with those crystals diffracted at very high resolution at the synchrotron facility. The crystals diffracted at good resolution at the inhouse facility, as seen in the statistics shown in Table 1. It is a pre-requisite to test in advance all crystals when traveling to the synchrotron facilities. We do this is to guarantee that those are protein crystals, and also to get some ideas about the resolution and the pre-characterization of the samples. Table 2 shows the data collection and refinement statistics of all model proteins diffracted at the synchrotron facility. As the table shows, these protein crystals were both perfectly thermo-protected and arrived at the synchrotron facilities without degradation.

Table 1. Data collection at an in-house X-ray diffraction facility and statistics of proteins (blanks) of lysozyme, glucose isomerase, xylanase and ferritin.

Data Collection Facility	**Inhouse X-ray Diffraction Facility**	**Inhouse X-ray Diffraction Facility**	**Inhouse X-ray Diffraction Facility**	**Inhouse X-ray Diffraction Facility**
Protein	**Lysozyme**	**Glucose Isomerase**	**Xylanase**	**Ferritin**
Wavelength (Å)	1.54	1.54	1.54	1.54
Space group	$P4_32_12$	I222	$P2_12_12_1$	F432
Unit cell dimensions	78.14, 78.14, 37.39	93.05, 98.28, 102.13	48.91, 58.39, 69.82	182.42, 182.42, 182.42
[*a*, *b*, *c* (Å)]	90,90,90	90,90,90	90, 90, 90	90,90,90
Resolution (Å)	39.20–1.45	35.41–1.70	40.06–1.00	50.00–2.00
No. of unique reflections	18,837	267,071	111,185	18,108
Completeness (%)	99.82 (100)	99.8 (98.7)	99.70 (95.1)	99.7 (100)
Redundancy	12.6(13.3)	5.2(4.8)	5.7 (2.9)	11.4 (15.2)
R_{merge} (%)	0.038 (0.71)	0.08 (0.37)	0.064 (0.871)	0.075 (0.57)
Mean $\langle I/\sigma(I)\rangle$	35.33(4.3)	11.1(3.)	33.4 (1.6)	12.0(3.1)

Table 2. Data collection and refinement statistics for lysozyme, glucose isomerase, xylanase and ferritin.

Data Collection Beamline	**XRD1 (Elettra)**	**XRD1 (Elettra)**	**XRD1 (Elettra)**	**XRD1 (Elettra)**
Protein	**Lysozyme**	**Glucose Isomerase**	**Xylanase**	**Ferritin**
Wavelength (Å)	0.9794	0.9794	0.9794	0.9794
Space group	$P\,4_32_12$	$I\,222$	$P\,2_12_12_1$	$F\,432$
Unit cell parameters (Å)	a = 78.45, b = 78.45, c = 37.21	a = 93.03, b = 98.56, c = 102.47	a = 48.98, b = 58.62, c = 69.90	a = 181.84, b = 181.84, c = 181.84
Resolution range (Å)	39.22–0.91 (0.94–0.91)	40.08–1.102 (1.141–1.102)	37.59–1.00 (1.036–1.00)	40.66–1.75 (1.81–1.75)
No. of reflections	835,727 (10,161)	1,168,535 (105,218)	667,833 (57,308)	984,926 (100,812)
No. of unique reflections	75,009 (3210)	185,699 (17,833)	108,893 (10,737)	26,552 (2469)
Multiplicity	11.1 (2.9)	6.3 (5.8)	6.1 (5.3)	37.1 (38.7)
Completeness (%)	99.59 (39.90)	98.36 (95.58)	99.73 (99.60)	98.85 (93.97)
Mean I/σ (I)	21.72 (0.20)	9.64 (0.70)	28.84 (4.58)	32.21 (1.86)
R_{merge} [1]	0.0414 (4.594)	0.0759 (2.433)	0.0370 (0.3304)	0.1127 (2.305)
R_{meas} [2]	0.0433 (5.403)	0.0827 (2.668)	0.0403 (0.3679)	0.1144 (2.336)
$CC_{1/2}$ [3]	100 (88)	99 (68)	99 (95)	88 (90)
Mosaicity (°)	1.3	1.2	0.6	2.2
Wilson B-factor (Å^2)	12.68	14.3	8.79	32.04
Refinement				
R_{work}/R_{free}	0.1582 (0.4441)/0.1876 (0.5569)	0.2547 (0.5306)/0.2582 (0.5569)	0.1394 (0.1509)/0.1684 (0.1859)	0.2309 (0.6569)/0.2541 (0.6351)
Working reflections	74,646 (3210)	185,400 (17,825)	108,816 (10,736)	26,252 (2446)
Testing reflections	3718 (170)	9110 (856)	5462 (551)	1293 (112)
Non-H atoms	1276	3072	2042	1557
Protein	129	390	190	171
Ligands	2	10	12	3
Water molecules	262	28	523	178
Mean B factors (Å^2)				
Protein	16.39	17.69	10.14	31.15
Ligands	14.11	17.70	16.48	67.71
Water molecules	37.85	28	35.36	41.98
rmsd bond lengths (Å)	0.009	0.008	0.006	0.007
rmsd angles (°)	1.4	1.33	1.36	1.05
Ramachandran plot statistics				
Favored	98.43%	97.14%	98.4%	97.63%
Outliers	0%	0.26%	0%	0.59%
Allowed	1.57%	2.60%	1.6%	1.78%

Statistics for the highest resolution shell are shown in parentheses.

$$R_{merge} = \frac{S_{hkl} S_i |I_i(hkl) - \{I(hkl)\}|}{S_{hkl} S_i I_i(hkl)} \quad (1)$$

$$R_{meas} = \sum_{hkl} \frac{(N-1)^{-\frac{1}{2}} \sum_i |I_i(hkl) - \{I(hkl)\}|}{\sum_{hkl} \sum_i I_i(hkl)} \quad (2)$$

where $I_i(hkl)$ is the intensity measured for the ith reflection and $(I_i(hkl))$ is the average intensity of all reflections with indices hkl.

$$CC_{1/2} \quad (3)$$

is the correlation coefficient between two random half datasets.

The following set of pictures (Figure 4) shows the best crystallization results of the model proteins transported in the aforementioned thermal protection devices (as shown in the data collection and refinement statistics of Table 2). The high-resolution electron-density map shown for the aromatic residues proves that the crystals diffracted the X-rays at very high resolution. Additionally, it can be seen that all protein crystals arrived at the synchrotron facilities without crystal structure damage.

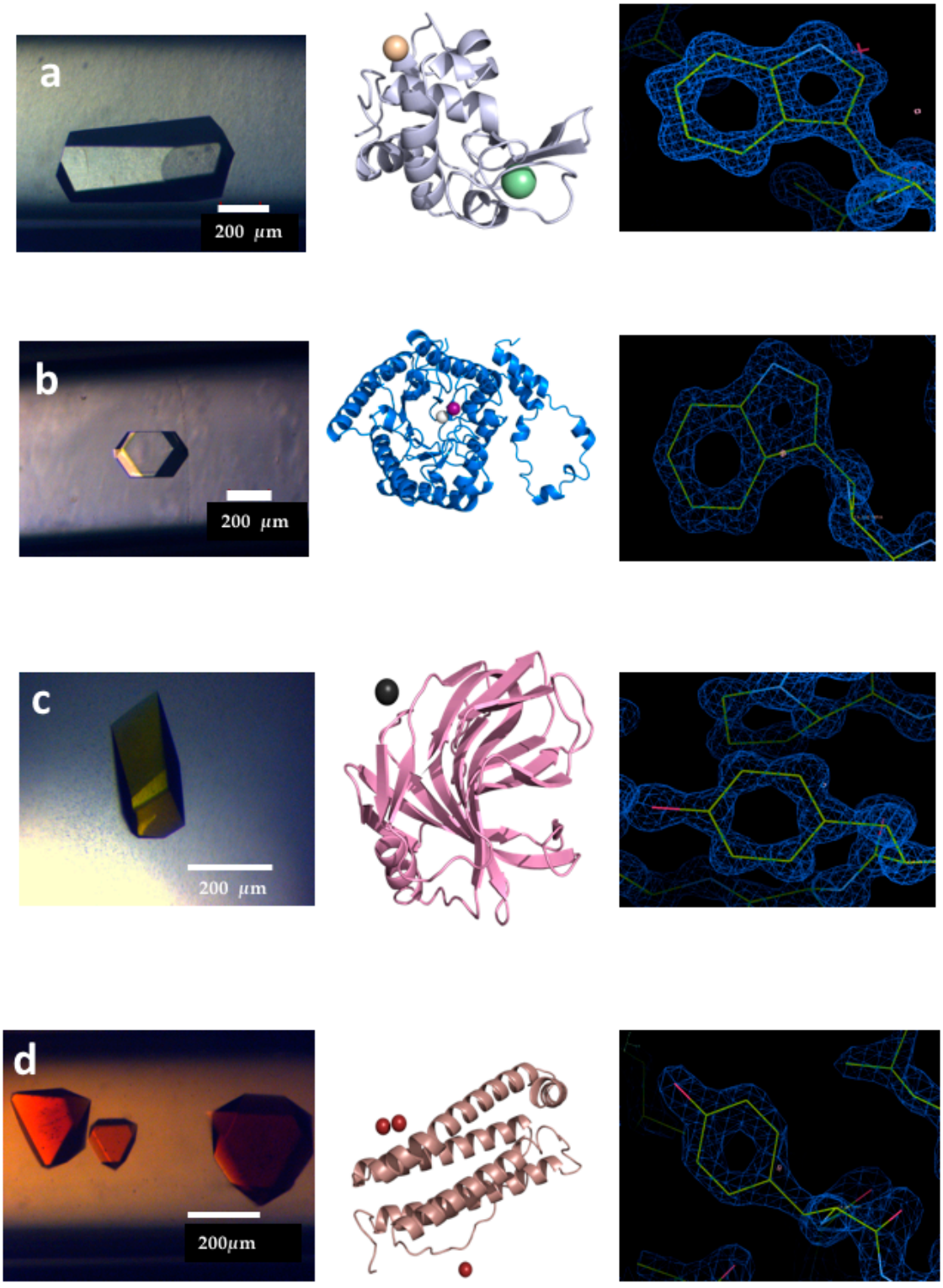

Figure 4. This shows the crystal shape and crystal structure as well as the high-resolution electron density map ($2F_0$–F_c) for (**a**) lysozyme, (**b**) glucose isomerase, (**c**) xylanase and (**d**) ferritin respectively. Contour level was 2.5–2.3 σ due to the high resolution reached.

We have also evaluated the crystallization of apo-transferrin, a protein involved in neurodegenerative diseases who is extremely sensitive to even the slightest change in temperature when crystallizing. This protein was used as thermal sensor to prove the efficiency of these devices.

Initially, the influence of temperature was investigated in our laboratory fixing crystallization experiments at different temperatures ranging from 12 to 22 °C. This was performed in a TG40 apparatus apparatus (Centeo BioSciences-Blacktrace, Royston, UK). Figure 5 shows pictures where the best temperature for the crystallization conditions was determined at 18 °C (Figure 5a). Any small change around this temperature provoked crystals dissolution and damage in the crystal structure (see Figure 5b). Additionally, a study about the influence of pH on protein crystallization was also performed (results not shown). This study showed that the apo-transferrin crystallizes at very specific pH value of 7.0. Crystals obtained at 18 °C were bigger than those obtained at 19 °C. A slight changes in temperature shifted to dissolution of protein crystals modifying the overall shape and homogeneity of apo-transferrin crystals. Figure 5c,d show crystal conservation over time experiment: We got beamtime assigned at the synchrotron facilities at the beginning of the spring. The mounting robot failed during the data collection at the synchrotron facility and the data collection was stopped. Then, those apo-transferrin crystals returned to Mexico for the next round at the synchrotron planned two months and a half later (in the summer) to be diffracted at the same facility. These crystals were preserved inside the thermal protection devices during two and half months-time prior to diffraction in the synchrotron. These crystals traveled again inside the thermal protection devices and diffracted the X-ray without any damage in the crystal structure. Figure 6 shows the X-ray crystal structure of apo-transferrin obtained at the best crystallization conditions as those shown in Figure 5a. The PDB code 2HAV was used for apo-transferrin to solve the 3D X-ray crystal structure for the molecular replacement.

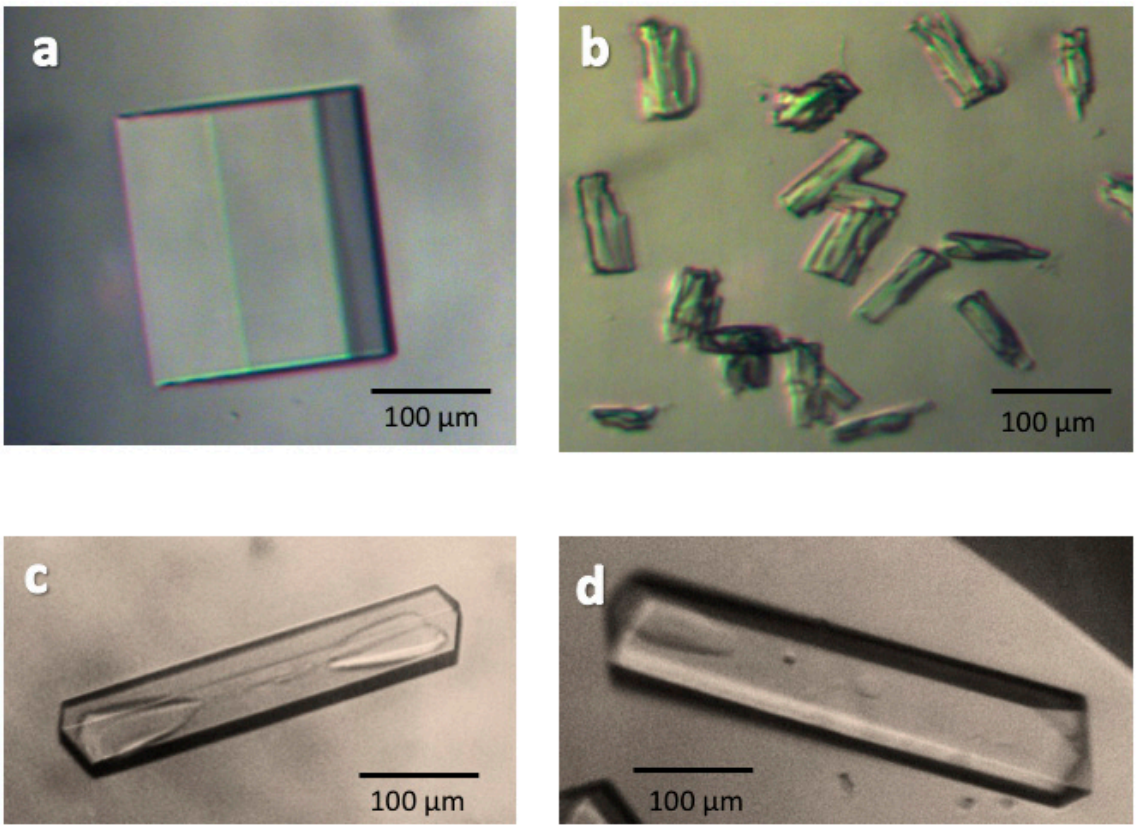

Figure 5. (**a**) Optimal temperature and crystallization conditions for apo-transferrin at 18 °C, (**b**) crystals grown at 19 °C were slightly dissolved. Crystal conservation over time: (**c**) Crystals grown during three days after crystallization; and (**d**) crystal observed after transportation (trip) to the synchrotron facility 2.5 months later. The crystals were preserved inside these devices and worked as thermal sensors.

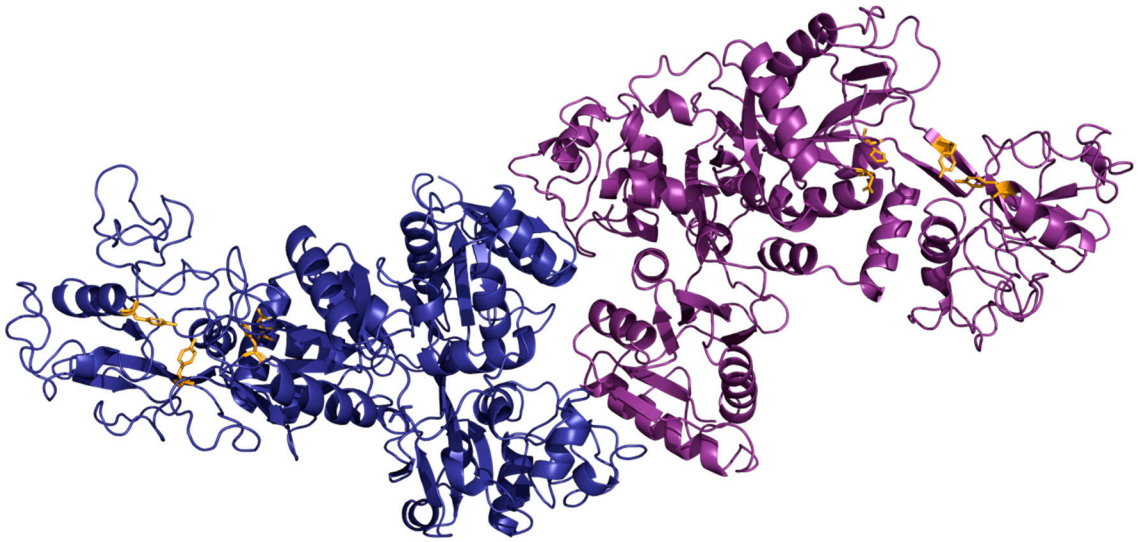

Figure 6. It shows the crystal structure of apo-transferrin; crystals diffracted up to 2.9 Å at the best temperature, keeping the optimal pH and appropriate cryo-protection conditions as described in the experimental part.

Table 3 shows the statistics of these apo-transferrin crystals when comparing two types of crystals, the first crystals were grown and diffracted at inhouse X-ray facility. Then, a second set of crystals grown at the same crystallization conditions, and were transported to the synchrotron facility. Again, we see that the crystal quality was preserved inside the thermal protection device compared to that crystal grown and diffracted at inhouse facilities. The quality of the crystal obtained at the synchrotron facility was better as it is usually the case of most of crystals tested in these facilities. However, we are not trying to compare the crystal quality here, but to emphasize that all crystals were properly transported and that they (due to the characteristics of the synchrotron facilities) diffracted at least at the same resolution, or even higher, than those taken to inhouse facilities.

Table 3. Apo-transferrin: Data collection and X-ray statistics.

	Inhouse X-ray Diffraction Facility	**Synchrotron Facility**
Wavelength (Å)	1.5418	0.9184
Resolution range (Å)	41.57–3.51 (3.63–3.51)	29.60–2.91 (2.99–2.91)
Space group	$P\,2_1\,2_1\,2_1$	$P\,2_1\,2_1\,2_1$
Unit cell (Å)	a = 84.99, b = 101.41, c = 200.327	a = 85.40, b = 101.60, c = 199.60
Total reflections	221,910	253,338 (13,314)
Unique reflections	22,370	37,976 (2411)
Multiplicity	9.9	6.7 (5.5)
Completeness (%)	99.9	98.8 (86.6)
Mean I/sigma(I)	1.9	12.20 (1.30)
R-merge	0.163	0.100 (0.728)
$CC_{1/2}$	69.6	99.8 (81.3)

We definitely encourage the use of these thermal devices when traveling or transporting protein crystals which are extremely sensitive to changes in temperature, by taking them directly to the synchrotron facility—where the crystals are stabilized for a few hours before opening these devices at the temperature of crystallization conditions for cryo-protecting or mounting them. This procedure will allow the same crystals resolution as those obtained in the crystallization room at inhouse X-ray facilities. The 3D X-ray crystal structure of apo-transferrin has been already reported, however the full structure of the four domains has never been crystallized completely. In this investigation we have

proven that the transportation of crystals (whereas by conventional dry Dewar or any other system) play a major role in the obtaining of quality crystals when low temperature is involved. In the majority of laboratories, most crystals usually are grown at 4 °C or 18 °C, this is why their transportation temperature has to be kept the same in order to guaranty the proper crystallization conditions. Our devices have proven their efficiency in keeping the crystals temperature in transportation, guarantying, therefore, their thermo-stability and their quality in the data-collection process. Based on these results, a temperature insulator like the one shown in here, opens up the possibility of a proper thermo-protection of the crystal structures when traveling, bettering, therefore, the quality of the obtained crystals. As far as we know this is the first time that such an approach has been dealt with from an investigations point of view and hope that they will enhance our future investigation results.

4. Conclusions

Based on these results, we can finally conclude that these three types of thermal protection devices are the most promising transportation items to the synchrotron facilities in order to preserve high protein crystal quality (as shown in the X-ray crystallographic analysis). However further experiments applying these devices to a variety of proteins extremely sensitive to changes in temperature need to be performed.

Author Contributions: A.F.-I., E.R., and Y.G. analyzed the crystallographic data of model proteins; A.M. and M.C.-C. performed the X-ray data collection at the synchrotron facilities; M.C.-C. and A.M. conceived and designed the experiments as well as wrote the manuscript. C.C.-E., performed the purification, crystallization experiments of apo-transferrin as well as their crystal structure resolution, she also acknowledges to SNI for the scholarship. D.N. and M.P., supported with the X-ray and analyzed the data at the synchrotron Elettra in Trieste Italy.

Acknowledgments: One of the authors (A.M.) acknowledges the support of DGAPA UNAM project PAPIIT No. IG200218 for this research. All authors acknowledge to the synchrotron ELETTRA for the X-ray facilities and data collection. Antonia Sanchez for the English revision of this manuscript.

Conflicts of Interest: "The authors declare no conflict of interest". Additionally, we state that "The founding sponsors had no role in the design of the study; in the collection, analyses, or interpretation of data; in the writing of the manuscript, and in the decision to publish the results".

References

1. Lorber, B.; Sauter, C.; Theobald-Dietrich, A.; Moreno, A.; Schellenberger, P.; Robert, M.C.; Capelle, B.; Sanglier, S.; Potier, N.; Giege, R. Crystal growth of proteins, nucleic acids, and viruses in gels. *Prog. Biophys. Mol. Biol.* **2009**, *101*, 13–25. [CrossRef] [PubMed]
2. Dauter, Z.; Wlodawer, A. Progress in Protein Crystallography. *Protein Peptide Lett.* **2016**, *23*, 201–210. [CrossRef]
3. Fuertes, G.; Banterlea, N.; Ruff, K.M.; Chowdhury, A.; Mercadante, D.; Koehler, C.; Kachala, M.; Girona, G.E.; Milles, S.; Mishra, A.; et al. Decoupling of size and shape fluctuations in heteropolymeric sequences reconciles discrepancies in SAXS vs. FRET measurements. *Proc. Natl. Acad. Sci. USA* **2017**, *114*, E6342–E6351. [CrossRef] [PubMed]
4. Sugiki, T.; Kobayashi, N.; Fujiwara, T. Modern Technologies of Solution Nuclear Magnetic Resonance Spectroscopy for Three-dimensional Structure Determination of Proteins Open Avenues for Life Scientists. *Comput. Struct. Biotechnol.* **2017**, *15*, 328–339. [CrossRef] [PubMed]
5. Kay, L.E. Nuclear magnetic resonance methods for high molecular weight proteins: A study involving a complex of maltose binding protein and beta-cyclodextrin. *Method Enzymol.* **2001**, *339*, 174–203.
6. Ovchinnikov, S.; Kim, D.E.; Wang, R.Y.R.; Liu, Y.; DiMaio, F.; Baker, D. Improved de novo structure prediction in CASP11 by incorporating coevolution information into Rosetta. *Proteins* **2016**, *84*, 67–75. [CrossRef] [PubMed]
7. Rambo, R.P.; Tainer, J.A. Super-resolution in solution X-ray scattering and its applications to structural systems biology. *Annu. Rev. Biophys.* **2013**, *42*, 415–441. [CrossRef] [PubMed]
8. Jolley, C.C.; Wells, S.A.; Fromme, P.; Thorpe, M.F. Fitting low-resolution Cryo-EM maps of proteins using constrained geometric simulations. *Biophys. J.* **2008**, *94*, 1613–1621. [CrossRef] [PubMed]

9. Stagno, J.R.; Liu, Y.; Bhandari, Y.R.; Conrad, C.E.; Panja, S.; Swain, M.; Fan, L.; Nelson, G.; Li, C.; Wendel, D.R.; et al. Structures of riboswitch RNA reaction states by mix-and-inject XFEL serial crystallography. *Nature* **2017**, *541*, 242. [CrossRef] [PubMed]
10. Liu, W.; Wacker, D.; Gati, C.; Won-Han, G.; James, D.; Wang, D.; Nelson, G.; Weierstall, U.; Katritch, V.; Barty, A.; et al. Serial Femtosecond Crystallography of G Protein-Coupled Receptors. *Science* **2013**, *342*, 1521–1524. [CrossRef] [PubMed]
11. Zander, U.; Cianci, M.; Foos, N.; Silva, C.S.; Mazzei, L.; Zubieta, C.; de Maria, A.; Nanao, M.H. Mergin of synchrotron serial crystallographic data by a genetic algorithm. *Acta Cryst.* **2016**, *D72*, 1026–1035.
12. Giege, R.; Mikol, V. Crystallogenesis of Proteins. *Trends Biotechnol.* **1989**, *7*, 277–282. [CrossRef]
13. Rosenberger, F. Protein crystallization. *J. Cryst. Growth* **1996**, *166*, 40–54. [CrossRef]
14. Mcpherson, A. Crystallization of Proteins by Variation of Ph or Temperature. *Methods Enzymol.* **1985**, *114*, 125–127. [PubMed]
15. Moller, J.; Schroer, M.A.; Erlkamp, M.; Grobelny, S.; Paulus, M.; Tiemeyer, S.; Wirkert, F.J.; Tolan, M.; Winter, R. The Effect of Ionic Strength, Temperature, and Pressure on the Interaction Potential of Dense Protein Solutions: From Nonlinear Pressure Response to Protein Crystallization. *Biophys. J.* **2012**, *102*, 2641–2648. [CrossRef] [PubMed]
16. Juarez-Martinez, G.; Garza, C.; Castillo, R.; Moreno, A. A dynamic light scattering investigation of the nucleation and growth of thaumatin crystals. *J. Cryst. Growth* **2001**, *232*, 119–131. [CrossRef]
17. Rosenberger, F.; Howard, S.B.; Sowers, J.W.; Nyce, T.A. Temperature-Dependence of Protein Solubility—Determination and Application to Crystallization in X-Ray Capillaries. *J. Cryst. Growth* **1993**, *129*, 1–12. [CrossRef]
18. Martinez-Caballero, S.; Cuellar-Cruz, M.; Demitri, N.; Polentarutti, M.; Rodriguez-Romero, A.; Moreno, A. Glucose Isomerase Polymorphs Obtained Using an Ad Hoc Protein Crystallization Temperature Device and a Growth Cell Applying an Electric Field. *Cryst. Growth Des.* **2016**, *16*, 1679–1686. [CrossRef]
19. Strelov, V.I.; Zakharov, B.G.; Bezbakh, I.Z.; Safronov, V.V.; Chernyshev, B.V.; Dutyshev, I.N. Implementation of Temperature-Controlled Method of Protein Crystallization in Microgravity. *Crystallogr. Rep.* **2018**, *63*, 149–153. [CrossRef]
20. Chen, R.Q.; Lu, Q.Q.; Cheng, Q.D.; Ao, L.B.; Zhang, C.Y.; Hou, H.; Liu, Y.M.; Li, D.W.; Yin, D.C. An ignored variable: Solution preparation temperature in protein crystallization. *Sci. Rep.* **2015**, *5*, 7797. [CrossRef] [PubMed]
21. Ferreira, C.; Crespo, R.; Martins, P.M.; Gales, L.; Rocha, F.; Damas, A.M. Small temperature oscillations promote protein crystallization. *CrystEngComm* **2011**, *13*, 3051–3056. [CrossRef]
22. Budayova-Spano, M.; Dauvergne, F.; Audiffren, M.; Bactivelane, T.; Cusack, S. A methodology and an instrument for the temperature-controlled optimization of crystal growth. *Acta Crystallogr. Sect. D Biol. Crystallogr.* **2007**, *63*, 339–347. [CrossRef] [PubMed]
23. Berg, M.; Urban, M.; Dillner, U.; Muhlig, P.; Mayer, G. Development and characterization of temperature-controlled microreactors for protein crystallization. *Acta Crystallogr. Sect. D* **2002**, *58*, 1643–1648. [CrossRef]
24. Junius, N.; Oksanen, E.; Terrien, M.; Berzin, C.; Ferrer, J.L.; Budayova-Spano, M. A crystallization apparatus for temperature-controlled flow-cell dialysis with real-time visualization. *J. Appl. Crystallogr.* **2016**, *49*, 806–813. [CrossRef] [PubMed]
25. Astier, J.P.; Veesler, S. Using Temperature To Crystalize Proteins: A. Mini-Review. *Cryst. Growth Des.* **2008**, *8*, 4215–4219. [CrossRef]
26. Snyder, R.C.; Veesler, S.; Doherty, M.F. The evolution of crystal shape during dissolution: Predictions and experiments. *Cryst. Growth Des.* **2008**, *8*, 1100–1101. [CrossRef]
27. Zhang, C.Y.; Yin, D.C.; Lu, Q.Q.; Guo, Y.Z.; Guo, W.H.; Wang, X.K.; Li, H.S.; Lu, H.M.; Ye, Y.J. Cycling Temperature Strategy: A Method to Improve the Efficiency of Crystallization Condition Screening of Proteins. *Cryst. Growth Des.* **2008**, *8*, 4227–4232. [CrossRef]
28. Juarez-Martinez, G.; Steinmann, P.; Roszak, A.W.; Isaacs, N.W.; Cooper, J.M. High-throughput screens for postgenomics: Studies of protein crystallization using microsystems technology. *Anal. Chem.* **2002**, *74*, 3505–3510. [CrossRef] [PubMed]

29. Kiefersauer, R.; Than, M.E.; Dobbek, H.; Gremer, L.; Melero, M.; Strobl, S.; Dias, J.M.; Soulimane, T.; Huber, R. A novel free-mounting system for protein crystals: Transformation and improvement of diffraction power by accurately controlled humidity changes. *J. Appl. Crystallogr.* **2000**, *33*, 1223–1230. [CrossRef]
30. Pareja-Rivera, C.; Cuellar-Cruz, M.; Esturau-Escofet, N.; Demitri, N.; Polentarutti, M.; Stojanoff, V.; Moreno, A. Recent Advances in the Understanding of the Influence of Electric and Magnetic Fields on Protein Crystal Growth. *Cryst. Growth Des.* **2017**, *17*, 135–145. [CrossRef]
31. De la Mora, E.; Flores-Hernandez, E.; Jakoncic, J.; Stojanoff, V.; Siliqi, D.; Sanchez-Puig, N.; Moreno, A. SdsA polymorph isolation and improvement of their crystal quality using nonconventional crystallization techniques. *J. Appl. Crystallogr.* **2015**, *48*, 1551–1559. [CrossRef]
32. Wally, J.; Halbrooks, P.J.; Vonrhein, C.; Rould, M.A.; Everse, S.J.; Mason, A.B.; Buchanan, S.K. The crystal structure of iron-free human serum transferrin provides insight into inter-lobe communication and receptor binding. *J. Biol. Chem.* **2006**, *281*, 24934–24944. [CrossRef] [PubMed]
33. Belaidi, A.A.; Bush, A.I. Iron neurochemistry in Alzheimer's disease and Parkinson's disease: Targets for therapeutics. *J. Neurochem.* **2016**, *139*, 179–197. [CrossRef] [PubMed]
34. Booyjzsen, C.; Scarf, C.A.; Moreton, B.; Portman, I.; Scrivens, J.H.; Costantini, G.; Sadler, P.J. Fibrillation of transferrin. *Bba-Gen. Subj.* **2012**, *1820*, 427–436. [CrossRef] [PubMed]
35. Apostolakis, S.; Kypraiou, A.M. Iron in neurodegenerative disorders: Being in the wrong place at the wrong time? *Rev. Neurosci.* **2017**, *28*, 893–911. [CrossRef] [PubMed]
36. Torronen, A.; Harkki, A.; Rouvinen, J. Three-dimensional structure of the endo 1,4-beta-xylanase II from Trichodema reesei: Two conformational states in the active site. *EMBO J.* **1994**, *13*, 2493–2501. [PubMed]
37. Lausi, A.; Polentarutti, M.; Onesti, S.; Plaisier, R.J.; Busetto, E.; Bais, G.; Barba, L.; Cassetta, A.; Campi, G.; Lamba, D.; et al. Status of the crystallography beamlines at Elettra. *Eur. Phys. J. Plus* **2015**, *130*, 1–8. [CrossRef]
38. Minor, W.; Cymborowski, M.; Otwinowski, Z.; Chruszcz, M. HKL-3000: The integration of data reduction and structure solution—From diffraction images to an initial model in minutes. *Acta Crystallogr. D* **2006**, *62*, 859–866. [CrossRef] [PubMed]
39. Kabsch, W. XDS. *Acta Cryst.* **2010**, *D66*, 125–132. [CrossRef] [PubMed]
40. Adams, P.D.; Afonine, P.V.; Bunkoczi, G.; Chen, V.B.; Davis, I.W.; Echols, N.; Headd, J.J.; Hung, L.W.; Kapral, G.J.; Grosse-Kunstleve, R.W.; et al. PHENIX: A comprehensive Python-based system for macromolecular structure solution. *Acta Crystallogr. D* **2010**, *66*, 213–221. [CrossRef] [PubMed]
41. Emsley, P.; Cowtan, K. Coot: Model-building tools for molecular graphics. *Acta Crystallogr. D* **2004**, *60*, 2126–2132. [CrossRef] [PubMed]
42. Afonine, P.V.; Grosse-Kunstleve, R.W.; Chen, V.B.; Headd, J.J.; Moriarty, N.W.; Richardson, J.S.; Richardson, D.C.; Urzhumtsev, A.; Zwart, P.H.; Adams, P.D. phenix.model_vs_data: A high-level tool for the calculation of crystallographic model and data statistics. *J. Appl. Crystallogr.* **2010**, *43*, 669–676. [CrossRef] [PubMed]
43. De Lano, W.L. *The PyMOL Molecular Graphics System*; DeLano Scientific LLC: San Carlos, CA, USA, 2002.